TISSUE ENGINEERING: Part A
Volume 17, Numbers 15 and 16, 2011

DOI: 10.1089/ten.tea.2010.0719

Fgf-18 Is Required for Osteogenesis But Not Angiogenesis During Long Bone Repair

Björn Behr, M.D.,[1,2] Michael Sorkin, M.D.,[1] Alina Manu, B.S.,[1] Marcus Lehnhardt, M.D.,[2] Michael T. Longaker, M.D., M.B.A.,[1] and Natalina Quarto, Ph.D.[1,3]

Bone regeneration is a complex event that requires the interaction of numerous growth factors. Fibroblast growth factor (Fgf)-ligands have been previously described for their importance in osteogenesis during development. In the current study, we investigated the role of *Fgf-18* during bone regeneration. By utilizing a unicortical tibial defect model, we revealed that mice haploinsufficient for *Fgf-18* have a markedly reduced healing capacity as compared with wild-type mice. Reduced levels of *Runx2* and *Osteocalcin* but not *Vegfa* accompanied the impaired bone regeneration. Interestingly, our data indicated that upon injury angiogenesis was not impaired in *Fgf-18*$^{+/-}$ mice. Moreover, other Fgf-ligands and *Bmp-2* could not compensate for the loss of *Fgf-18*. Finally, application of FGF-18 protein was able to rescue the impaired healing in *Fgf-18*$^{+/-}$ mice. Thus, we identified *Fgf-18* as an important mediator of bone regeneration, which is required during later stages of bone regeneration. This study provides hints on how to engineering efficiently programmed bony tissue for long bone repair.

Introduction

Fracture healing requires the interplay of numerous growth factors to conduct different events during repair such as inflammation and angiogenesis, callus formation, and remodeling of the bone. Interestingly, fracture healing is thought to recapitulate aspects of skeletal development,[1,2] which opens up prospects to study fracture healing with a developmental lens. The fibroblast growth factor (Fgf) family and their receptors have been implicated in the regulation of numerous processes during skeletal development. For instance, depletion of *Fgf-2* resulted in decreased bone mass and bone formation in femurs postnatally,[3] depletion of *Fgf-9* in delayed vascularization and chondrocyte hypertrophy[4] and depletion of *Fgf-18* in smaller cranial vaults, deformed thoracic cavities, and shortened long bones.[5,6] Besides effects on osteogenesis *in vivo*, *Fgf-18* was also found to block chondrocyte proliferation[5,6] through activation of *Fgfr3*.[7] Of note, *Fgf-18* homozygotic mice *Fgf-18* die perinatally. Moreover, various skeletal syndromes are associated with activating mutations in the fibroblast growth factor receptors (FGFR) 1–3, such as craniosynostosis[8–10] or chondrodysplasias due to mutations in FGFR3,[11–13] which highlights the importance of Fgfs in skeletal pathology. In a recent characterization of Fgfs expression levels during repair of nonstable tibial fractures, a different temporal activation of a cluster of *Fgf* genes was identified.[14] Moreover, we have previously demonstrated that bone regeneration is impaired in *Fgf-9*$^{+/-}$ mice through decreased osteogenesis and angiogenesis.[15] Among the 23 members of Fgf family, *Fgf-18* is unique in consideration of the fact that is expressed by perichondrial cells and regulated by *Runx2*, a master gene of skeletogenesis.[16] First described in 1998,[17,18] *Fgf-18* is considered to inhibit chondrocyte proliferation and hypertrophy and promote differentiation of osteoblasts.[5,6] Further, it has been proposed that *Fgf-18* is a combined target of the canonical Wnt-pathway and *Runx2*, conducting the pro-osteogenic effects of these transcription factors.[19]

Given this compelling evidence for the importance of *Fgf-18* during skeletal development, in the current study we investigated the role of *Fgf-18* in bone regeneration.

Materials and Methods

Skeletal injuries

All experiments using animals were performed in accordance with Stanford University Animal Care and Use Committee Guidelines. Ten- to 12-week-old age- and sex-matched *Fgf-18*$^{+/-}$ and C57/Bl6 wild-type (WT) littermates were used for all studies. *Fgf-18*$^{+/-}$ mice were previously described[6] and kindly provided by Dr. David Ornitz (Washington University, St. Louis, MO). Genotyping was

[1]Hagey Laboratory, Department of Surgery, Stanford University School of Medicine, Stanford, California.
[2]BG-Unfallklinik Ludwigshafen, Department of Plastic- and Handsurgery, University of Heidelberg, Heidelberg, Germany.
[3]Department of Structural and Functional Biology, University of Naples Federico II, Complesso M. S. Angelo, Napoli, Italy.

performed by polymerase chain reaction (PCR) analysis on genomic DNA. Tibia injures were performed as previously described.[15] Briefly, after deeply anesthezing the mice, with an intraperitoneal injection of 100 mg/kg ketamine, 20 mg/kg xylazine, and 3 mg/kg acetopromazine the right legs were shaved and the skin was disinfected. Then, an incision was performed over the proximal medial diaphysis, followed by a division of the anterior tibial muscle. The medial surface of the tibia was exposed and the periosteum preserved. A unicortical defect was created with a 1 mm drill bit under constant irrigation. The anterior tibial muscle was reapproximated, the skin was closed, and mice were allowed to recover. Postoperative pain control was achieved by administration of 0.1 mg/kg buprenorphine. Mice were sacrificed after 3, 5, and 7 days, which represent the time points of inflammation/angiogenesis, hard callus formation, and remodeling. For rescue or gain-of-function experiments, defects were either treated with a 1-mm-diameter collagen sponge (Helistat; Integra Lifesciences Corporation, Plainsboro, NJ) soaked with phosphate-buffered saline (PBS) as control or with a collagen sponge soaked with 2 μg of FGF-18 (Santa Cruz Biotechnologies, Santa Cruz, CA) or vascular endothelial growth factor A (VEGFA) (R&D Systems, Minneapolis, MN) Sponges were inserted in the defects and filled out the generated bone marrow space.

Histology and immunohistochemistry

After 3, 5, and 7 days postoperatively, tibias were harvested and fixed in 4% paraformaldehyde overnight, decalcified, and paraffin embedded. Between five and eight animals were chosen for each time point and tibias were longitudinally sectioned at 9 μm. The 1 mm defect area was represented in about 60 sections. To evaluate new bone formation, every sixth slide was stained with Aniline blue, which detects the osteoid matrix or with hematoxylin and eosin according to standard procedures. Sections were photographed with a Leica digital imaging system at 5× and evaluated with Photoshop (Adobe, San Jose, CA). All images were cropped with a rectangular that covered the entire defect area (1×10^6 pixels). The selection of aniline blue-positive pixels was partially automated with the magic wand tool (tolerance: 60, no-contiguous). Cortical surfaces or bone chips from the drill injuries were manually deselected. The number of positive pixels was recorded and an average for each tissue sample was generated. Thereafter, averages for each group were calculated.

For immunohistochemistry, antigen retrieval was performed by incubating slides with Proteinase K (Sigma Aldrich, St. Louis, MO) at 37°C for 10 min. Primary antibodies against VEGFA (Lifespan Biosciences, Seattle, WA) were used at dilution of 1:100 and platelet endothelial cell adhesion molecule (PECAM) (Pharmingen, San Diego, CA) at dilution of 1:400. Antibodies against Runx2 and Osteocalcin (Santa Cruz Biotechnology) were used at dilution of 1:50. A rabbit or rat biotinylated secondary antibody followed by the AB reagent and NovaRed (Vector Laboratories, Burlingame, CA) were used for detection. Rabbit and rat IgG (Calbiochem, La Jolla, CA), used as negative controls, did not produce any staining (data not shown). Immunohistochemistry against anti-proliferative cell nuclear antigen (PCNA), was performed using a kit according to the manufacturer's instructions (Invitrogen, Carlsbad, CA). Results were obtained from at least three animals per time point, and immunohistochemistry was carried out in duplicates. PCNA-positive cells or vessels, indicated by round or oval PECAM-positive structures containing a lumen, were counted within the defect areas by two blinded independent examiners at 20× magnification. Results are presented as mean ± standard deviation. Tartrate-resistant acid phosphatase (TRAP) staining was performed using a leukocyte acid phosphatase kit (Sigma, St. Louis, MO).

Microcomputed tomography imaging

Microcomputed tomography (μCT) was performed, using a high-resolution MicroCAT II™ (ImTek Inc., Knoxville, TN) small animal imaging system, with the following settings: X-ray voltage of 80 kVp, anode current of 500 μA, and an exposure time of 500 ms for each of the 360 rotational steps. The two-dimensional projection images were used to reconstruct tomograms with a Feldkamp algorithm, using a commercial software package (Cobra EXXIM; EXXIM Computing Corp., Livermore, CA), resulting into a resolution of 80 μm. The duration of one scan was 9.5 min. Three-dimensional recon-

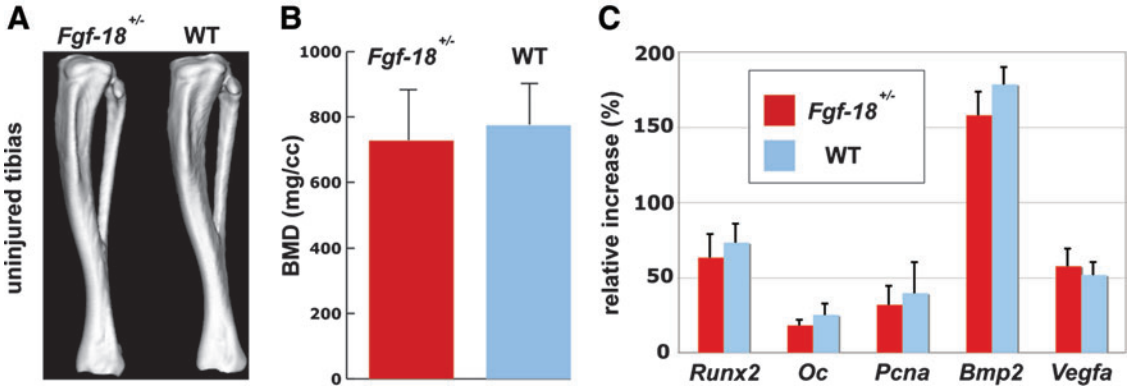

FIG. 1. No apparent differences in *Fgf-18*$^{+/-}$ and WT tibia. **(A)** Computed tomography scans of uninjured *Fgf-18*$^{+/-}$ and WT tibia revealed no obvious differences in shape. **(B)** Measurement of bone mineral density revealed no significant difference between *Fgf-18*$^{+/-}$ and WT tibia. **(C)** Quantitative real-time PCR analysis did not show differences in the gene expression profile for osteogenic, proliferative, and vascular markers. BMD, bone mineral density; Oc, osteocalcin; PCR, polymerase chain reaction; WT, wild type. Color images available online at www.liebertonline.com/tea

structions were generated by MicroView software (GE Healthcare, London, Canada). Each mouse was scanned with a CT-phantom (GE Healthcare), containing air bubble, water, and hydroxyapatite rod, which served for calibration of each scan. For determining bone mineral density (BMD), standardized regions in the diaphysis of the tibias were chosen and analyzed with the BMD tool in MicroView. The threshold range was set between 900 and 3500. The software automatically performed data analysis and calculations. Measurements were performed on four mice of each strain.

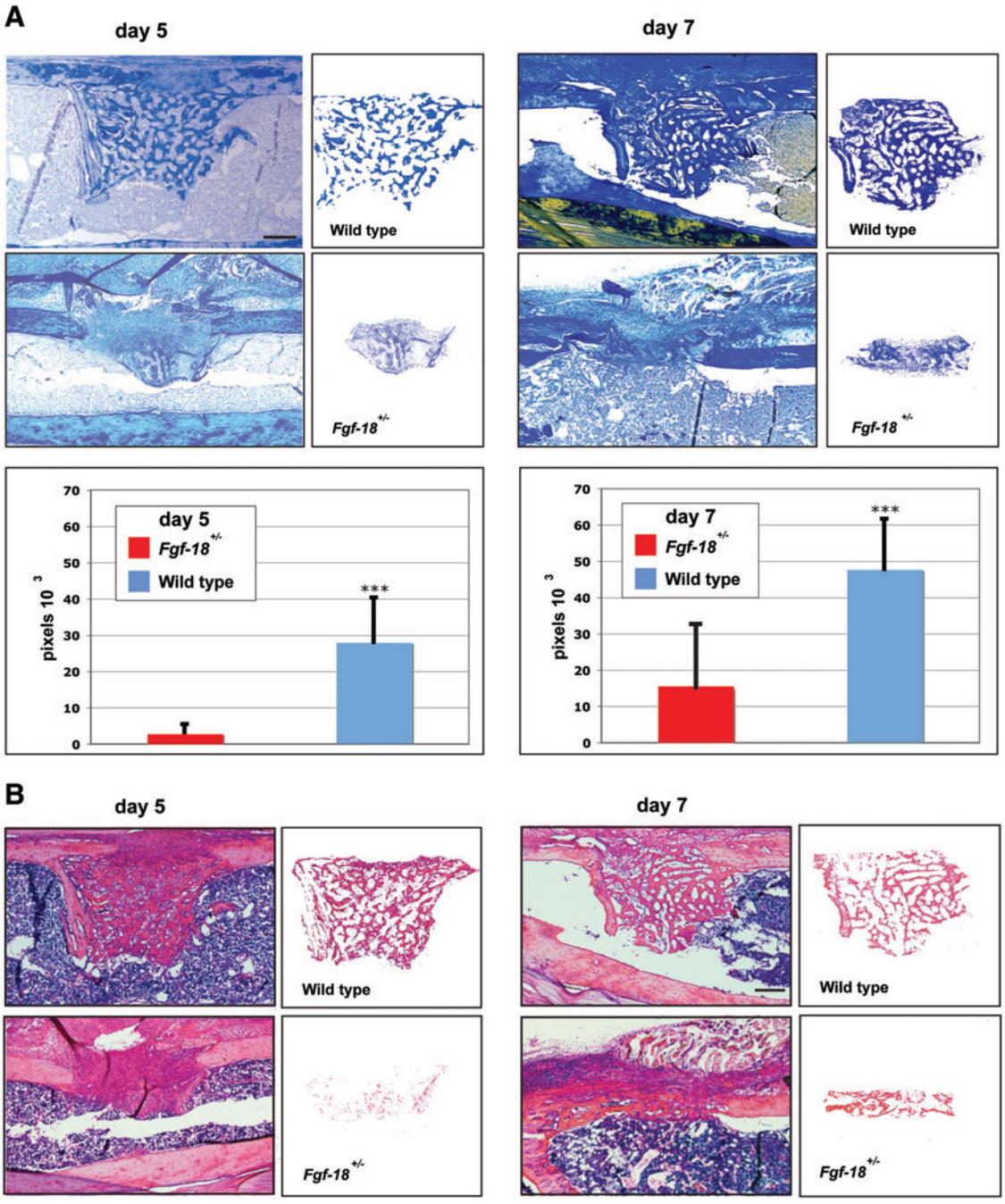

FIG. 2. Bone regeneration is impaired in *Fgf-18*$^{+/-}$ tibia. **(A)** Aniline blue staining of unicortical tibial defects revealed markedly impaired bone regeneration in *Fgf-18*$^{+/-}$ as compared with WT tibia at days 5 and 7 (upper panels). Histomorphometry performed on aniline blue-stained slides revealed a marked impairment of bone regeneration in *Fgf-18*$^{+/-}$ mice at both time points. ***$p < 0.0005$. **(B)** Hematoxylin and eosin staining of adjacent defects of *Fgf-18*$^{+/-}$ and WT tibia at days 5 and 7 paralleled these findings. **(C)** real-time-PCR (RT-PCR) analysis time course of *Runx2*, *Osteocalcin*, and *Vegfa* harvested from defects of *Fgf-18*$^{+/-}$ and WT tibia. **(D)** Quantitative RT-PCR analysis of *Fgf-2*, *-9*, and *-18* and *Bmp2*. *$p < 0.05$ and **$p < 0.005$. **(E)** Immunohistochemistry for PCNA, Runx2, and Osteocalcin in *Fgf-18*$^{+/-}$ and WT mice. No differences were observed in staining for PCNA; however, reduced immunoreactivity for Runx2 and Osteocalcin were observed in defects of *Fgf-18*$^{+/-}$ tibia. **(F)** Quantification of PCNA-positive cells revealed no statistical differences in proliferation between *Fgf-18*$^{+/-}$ and WT defects. Scale bars: **(A, B)** 200 μm, **(E)** 50 μm. PCNA, proliferative cell nuclear antigen. Color images available online at www.liebertonline.com/tea

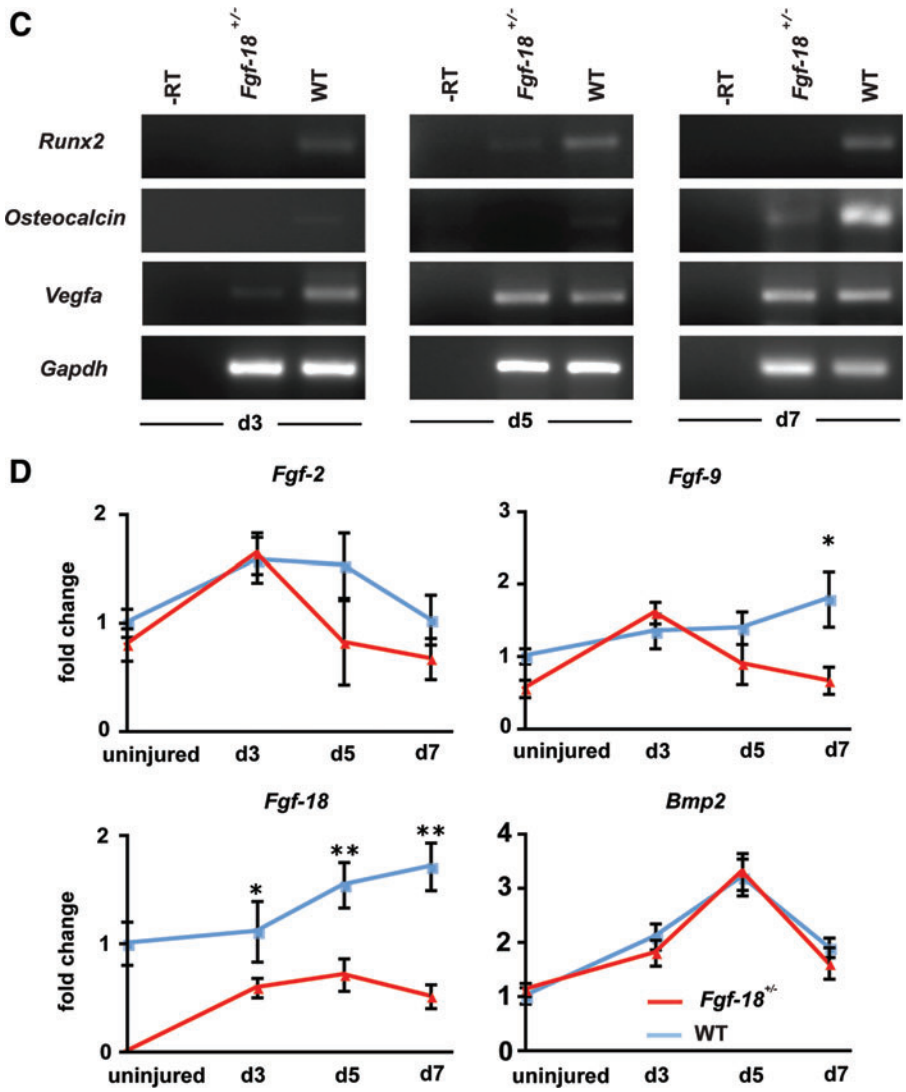

FIG. 2. (Continued).

μCT-angiographies

To assess neovascularization of bone defects in *Fgf-18*$^{+/-}$ and WT mice, animals underwent systemic perfusion with a radio-opaque contrast agent as previously described.[15,20] Briefly, 7 days after the creation of unicortical tibial defects, mice were deeply anesthetized, the thoracic cavity was opened, and the heart was exposed. The left ventricle was punctured, the right atrium incised, and the entire vascular system was flushed with normal saline using a 22G catheter. Then, Microfil MV-120 (Flow Tech, Inc Carver, MA) was injected until the entire vascular system was reliably perfused. After polymerization for 2 h at room temperature, tibias were harvested, fixed overnight in 10% neutral buffered formalin, and decalcified in 19% ethylenediaminetetraacetic acid. Samples were processed for imaging by Numirabio company (www.numirabio.com) and underwent μCT scanning (μCT40; ScanCo Medical, Zurich, CH) with the following parameters: 10 μm isotropic voxel resolution at 200 ms exposure time, 2000 views, and 5 frames per view. The μCT-generated DICOM files were converted into a file format compatible with the segmentation software Seg3D (Scientific Computing and Imaging Institute, University of Utah, Salt Lake City, UT). A consistent threshold was used across the samples to extract the vasculature from the data sets using Seg3D. After the samples were imaged, measurements were made on the actual samples to determine the area of damage. For quantification of the neovascularization, the voxel count associated with the region of interest was obtained after the segmentation process; that is, the number of voxels associated with the vasculature were counted using Seg3D. The voxel count was then multiplied by the voxel resolution cubed to obtain volume measurements.

RNA isolation, RT-PCR, and quantitative RT-PCR

RNA isolation was performed as previously described.[15] For RNA isolation, tibial defects of eight mice for each group were harvested, tibias were skeletonized, and defects were excised and homogenized in Trizol (Invitrogen). RNA was purified according to the manufacturer's protocol. Purified RNA was treated with DNAse I (Ambion, Austin, TX) to clear genomic DNA and reverse transcribed using the SuperScript First Strand Synthesis System (Invitrogen). Real-time (RT)-PCR

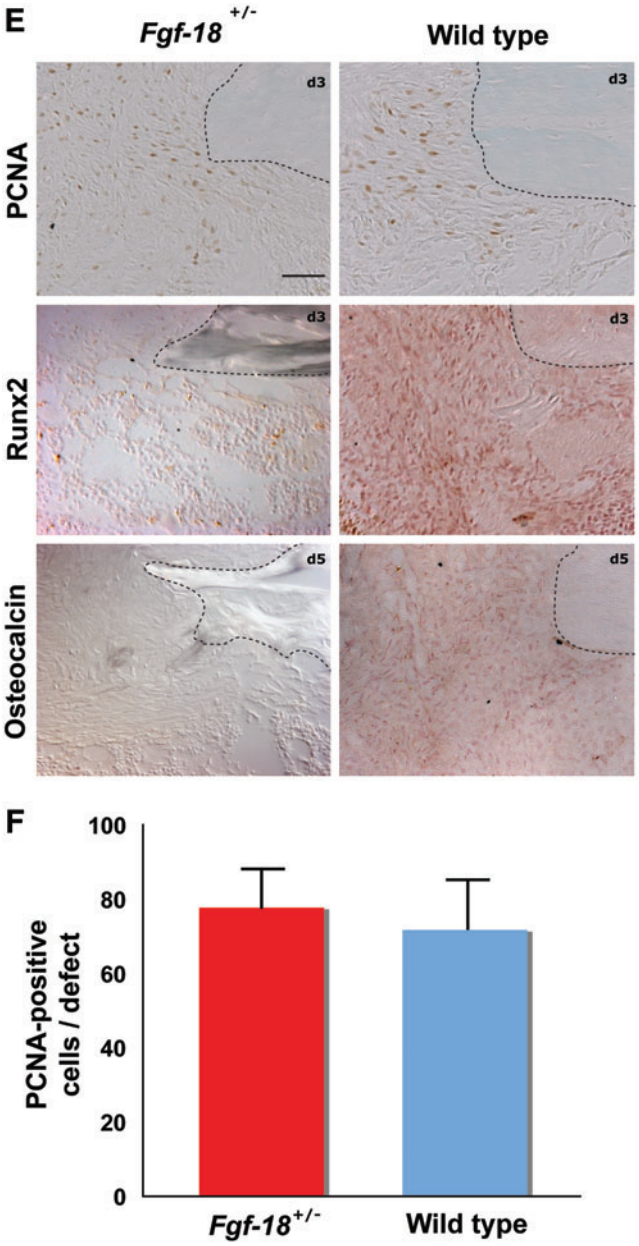

FIG. 2. (Continued).

and quantitative RT-PCR (QRT-PCR) were performed as previously described.[15,21]

Statistical analysis

Student's *t*-test was used for statistical analyses. A *p*-value < 0.05 was considered statistically significant.

Results

Fgf-18$^{+/-}$ *mice tibia did not display an overt phenotype*

As first we evaluated, whether tibias of *Fgf-18*$^{+/-}$ mice exhibited any gross phenotypic differences. CT-scans of *Fgf-18*$^{+/-}$ and WT mice did not reveal any noticeable differences (Fig. 1A). BMDs were in a similar range and were not statistically different (*Fgf-18*$^{+/-}$: 730 ± 155 mg/cc; WT: 774 ± 128 mg/cc) (Fig. 1B). QRT-PCR analysis of diaphysis of *Fgf-18*$^{+/-}$ and WT mice tibia did not reveal significant differences in the gene expression levels of osteogenic markers such as *Runx2* and *Osteocalcin* as well as proliferative and pro-osteogenic genes, like *Pcna* and *Bmp-2* and the angiogenic gene *Vegfa* (Fig. 1C).

Bone regeneration is impaired in Fgf-18$^{+/-}$ *mice*

To evaluate the bone regeneration capacity of *Fgf-18* haploinsufficient mice, *Fgf-18*$^{+/-}$ and WT mice underwent a tibial unicortical defect procedure, which represents an intramembranous healing model. Bone regeneration rates were determined during the hard callus (5 days postoperatively) and remodeling phase (7 days postoperatively). Aniline Blue staining revealed that new bone formation in *Fgf-18*$^{+/-}$ mice was significantly impaired as compared with WT mice (Fig. 2A). These findings were also confirmed by hematoxylin and eosin staining on adjacent slides (Fig. 2B). Histomorphometry indicated that in *Fgf-18*$^{+/-}$ mice bone formation rate was 90% reduced at postoperative day 5 and 67% reduced at postoperative day 7 as compared with WT mice ($^*p < 0.0005$). The severe impairment of bone regeneration in *Fgf-18*$^{+/-}$ mice prompted us to investigate, whether the expression of osteogenic genes were affected during the phases of healing. Indeed, expression of *Runx2*, an early marker of osteogenic differentiation, as well as, *Osteocalcin*, a late osteogenic marker, was lower at postoperative days 3, 5, and 7 in *Fgf-18*$^{+/-}$ compared with WT mice defects (Fig. 2C). In contrast, expression levels of *Vegfa* were lower in *Fgf-18*$^{+/-}$ mice only at postoperative day 3, but similar to WT defects at postoperative days 5 and 7 (Fig. 2C). QRT-PCR analysis of three pro-osteogenic Fgf ligands (*Fgf-2*, *-9*, and *-18*) revealed low levels of *Fgf-2* and *Fgf-9* in uninjured *Fgf-18*$^{+/-}$ tibia, whereas levels of *Fgf-18* were not detectable in uninjured *Fgf-18*$^{+/-}$ tibia (Fig. 2D). Interestingly, in *Fgf-18*$^{+/-}$ defects, *Fgf-2* and *Fgf-9* genes were upregulated to levels similar to WT defects at postoperative day 3 and not significantly different from WT defects with the exception of lower levels of *Fgf-9* in *Fgf-18*$^{+/-}$ defects at day 7. In sharp contrast and as expected, levels of *Fgf-18* expression were significantly lower in haploinsufficient *Fgf-18* defects than WT, at all time points analyzed. Interestingly, expression levels of *Bmp-2*, the prototypical osteogenic Bmp, were not impaired in tibial injuries of *Fgf-18*$^{+/-}$ mice (Fig. 2D). Moreover, immunohistochemistry for PCNA revealed similar staining in *Fgf-18*$^{+/-}$ and WT defects at postoperative day 3, thus suggesting that cell proliferation was not a limiting factor responsible for the impaired healing in *Fgf-18*$^{+/-}$ mice (Fig. 2E, F). However, immunoreactivity of Runx2 at postoperative day 3 and Osteocalcin at postoperative day 5 were lower in *Fgf-18*$^{+/-}$ defects than in WT defects, thereby mirroring the gene expression data.

Angiogenesis is not impaired in Fgf-18$^{+/-}$ *tibial defects*

To elucidate how *Fgf-18* might affect bone regeneration, we investigated the impact of *Fgf-18* haploinsufficency on angiogenesis, a crucial event during the inflammation phase of fracture healing. Gene expression analysis indicated that expression of *Vegfa* was only mildly impaired during the inflammation stage (Fig. 2B). As a next step to investigate angiogenesis in *Fgf-18*$^{+/-}$ and WT defects, we performed

immunohistochemistry for PECAM-1 (CD31), an endothelial marker. As shown in Figure 3A, an intense staining and vessel formation were observed in both *Fgf-18*$^{+/-}$ and WT defects at postoperative day 3. Moreover, immunohistochemistry for VEGFA paralleled this finding, revealing similar VEGF staining in both *Fgf-18*$^{+/-}$ and WT defects (Fig. 3A). Quantification of the vessel numbers within the defects as indicated by positive PECAM-1 stain and their round or oval structure revealed no statistical differences between *Fgf-18*$^{+/-}$ and WT defects (Fig. 3B). To further validate that angiogenesis was not impaired in *Fgf-18*$^{+/-}$ mice, we performed μCT angiography of the defects at postoperative day 7 (Fig. 3C). Quantification of both vessel volume (309 μm^3 in *Fgf-18*$^{+/-}$ and 332 μm^3 in WT mice) (Fig. 3D) and vessel surface area (15.4 mm^2 in *Fgf-18*$^{+/-}$ and 16.1 mm^2 in WT mice) (Fig. 3E) revealed similar levels in both defects. Taken together, the above results strongly suggest that angiogenesis is not impaired in *Fgf-18*$^{+/-}$ tibial defects.

Bone remodeling is impaired in Fgf-18$^{+/-}$ *tibial defects*

Having demonstrated an impairment of osteogenesis, but not angiogenesis in *Fgf-18*$^{+/-}$ mice, we sought to examine the effect of *Fgf-18* on osteoclastogenesis. Staining for TRAP at day 7 revealed little staining in *Fgf-18*$^{+/-}$ tibial defects, whereas in WT defects, staining for TRAP was strong and found in the regenerating part of the bone (Fig. 4). This observation indicated that remodeling in *Fgf-18*$^{+/-}$ tibial defects was impaired; however, it must be noted that this effect could also be due to the decreased amount of bone regeneration occurring in *Fgf-18*$^{+/-}$ tibial defects.

Bone regeneration in Fgf-18$^{+/-}$ *tibial defects can be rescued with FGF-18*

Finally, we investigated whether application of VEGFA or FGF-18 could rescue the impaired healing of tibial defects in *Fgf-18*$^{+/-}$ mice. VEGFA, well known for the capability to

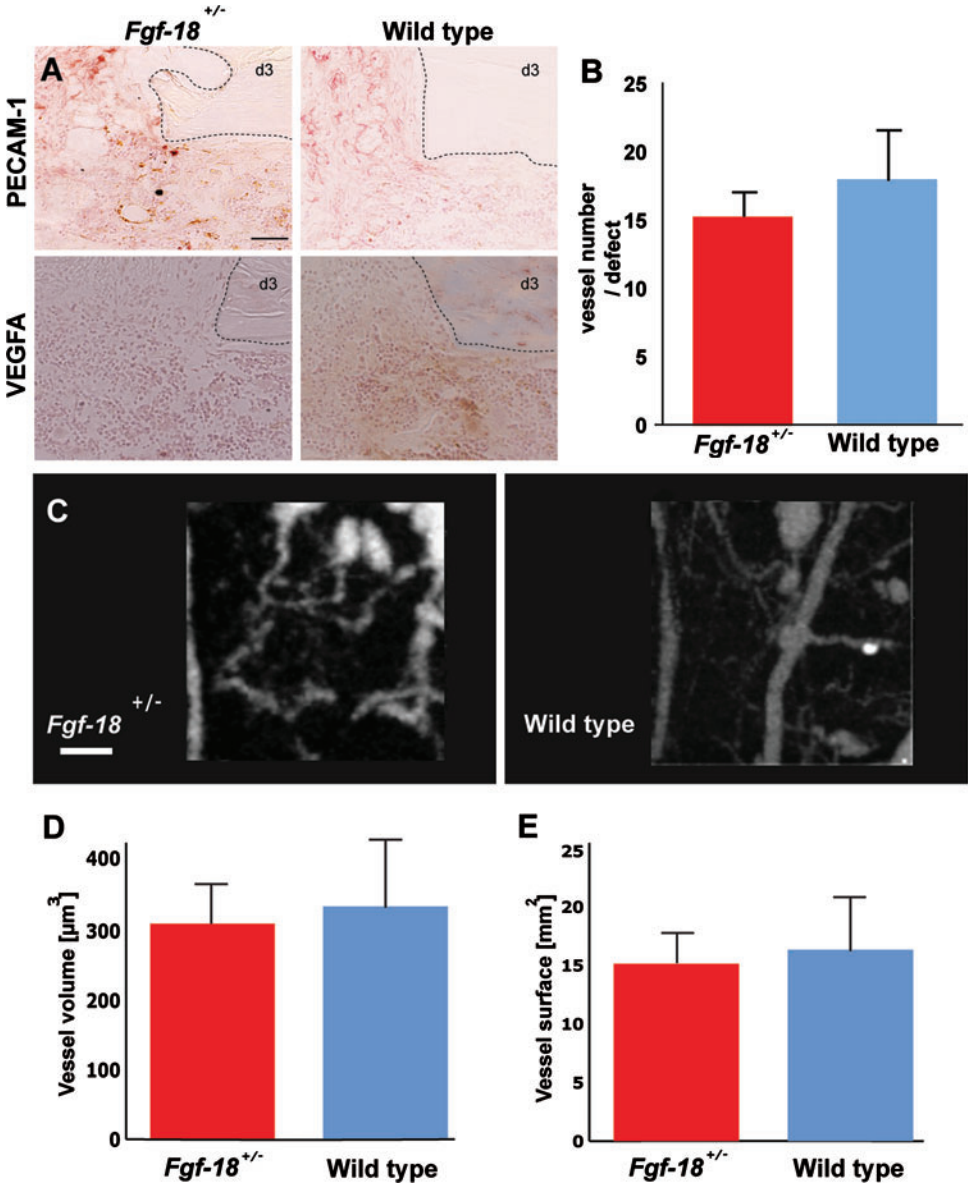

FIG. 3. Angiogenesis is not impaired in *Fgf-18*$^{+/-}$ tibia. **(A)** At day 3 immunohistochemistry for PECAM-1 and vascular endothelial growth factor A (VEGFA) did not reveal differences between *Fgf-18*$^{+/-}$ and WT tibia. **(B)** Quantification of vessel numbers as indicated by PECAM staining revealed no statistical differences between *Fgf-18*$^{+/-}$ and WT defects. **(C)** Microcomputed tomography-angiography of *Fgf-18*$^{+/-}$ and WT tibial defects at 7 day postoperatively. **(D)** Quantification of the vessel volume and **(E)** vessel surface area in the defects of *Fgf-18*$^{+/-}$ and WT mice did not reveal significant differences between the two groups. Scale bars: **(A)** 50 μm, **(C)** 200 μm. Dotted lines indicate the bony edges of the defects. PECAM, platelet endothelial cell adhesion molecule. Color images available online at www.liebertonline.com/tea

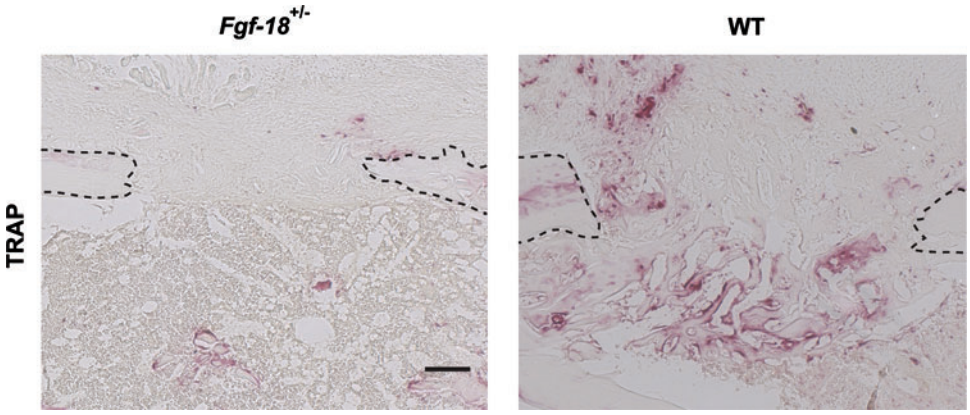

FIG. 4. Osteoclastogenesis is impaired in *Fgf-18*$^{+/-}$ tibia. Tartrate resistant acid phosphatase (TRAP) staining of *Fgf-18*$^{+/-}$ and WT tibial defects at 7 day postoperatively revealed a marked decrease in staining in *Fgf-18*$^{+/-}$ tibial defects. Scale bar: 200 μm. Dotted lines indicate the bony edges of the defects. Color images available online at www.liebertonline.com/tea

induce angiogenesis, has been previously demonstrated to accelerate osteogenesis.[15,22] After 7 days, no improvement of bone regeneration could be achieved by application of VEGF (2 μg)-soaked collagen sponges. Likewise, application of PBS-soaked collagen sponges as control did not accelerate bone regeneration in *Fgf-18*$^{+/-}$ tibial defects (Fig. 5A). In contrast, application of FGF-18 protein rescued defects in *Fgf-18*$^{+/-}$ mice (Fig. 5A). Quantification of bone regeneration revealed that application of FGF-18 to *Fgf-18*$^{+/-}$ tibial defects increased bone regeneration by 744% as compared with PBS alone and 1105% as compared with treatment with VEGFA ($p < 0.0005$ for both) (Fig. 5B). The rescue of bone regeneration in *Fgf-18*$^{+/-}$ tibial defects encouraged us to test the effects of FGF-18 in WT defects. Application on WT defects of collagen sponges soaked with FGF-18 slightly increased bone healing as compared with untreated WT defects, although this trend was not statistically significant (Fig. 5C). However, bone regeneration with FGF-18 in WT defects was significantly increased as compared with PBS-soaked collagen sponges ($p < 0.05$).

Discussion

The coming of regenerative medicine age has empowered tissue engineering as major discipline aimed to define and optimize techniques for regenerating tissues and organs. In

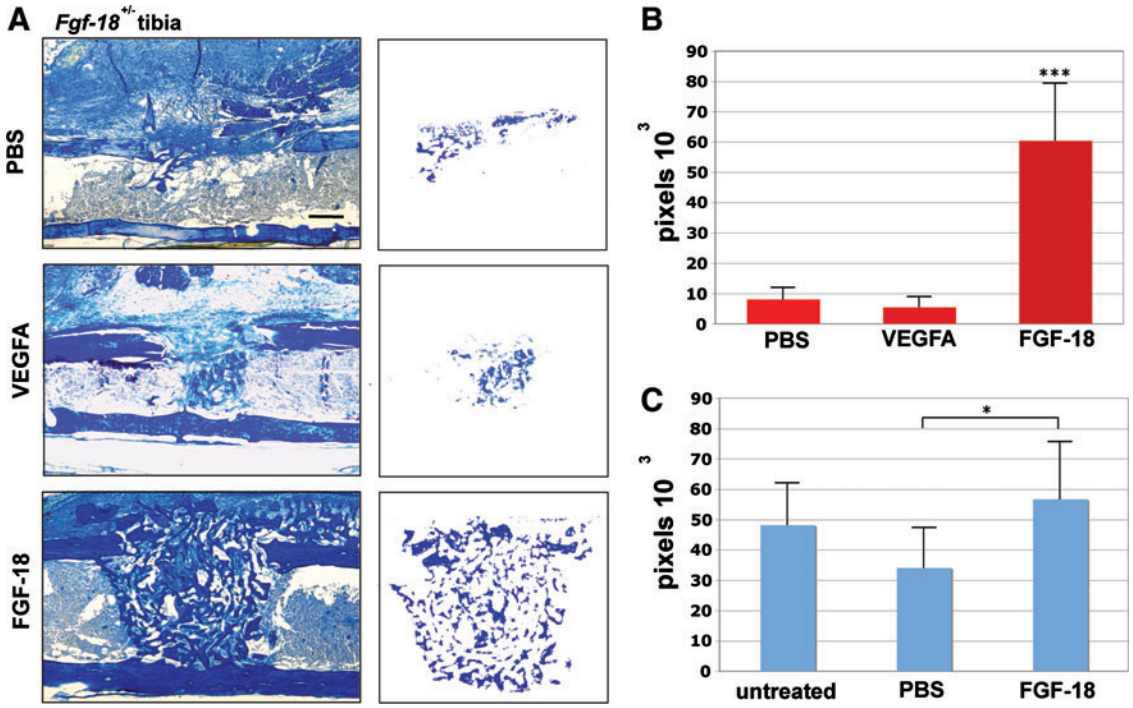

FIG. 5. Rescue of *Fgf-18*$^{+/-}$ tibial defects by application of FGF-18 but not VEGF. **(A)** Aniline blue staining of *Fgf-18*$^{+/-}$ tibial defects treated with phosphate-buffered saline (PBS), 2 μg VEGFA, or 2 μg FGF-18 7 days postoperatively. The injury site is segregated to the right column. Scale bar: 200 μm. **(B)** Histomorphometry revealed rescue of *Fgf-18*$^{+/-}$ tibial defects with FGF-18 protein but not with PBS or VEGFA, ***$p < 0.0005$. **(C)** Histomorphometry of untreated WT defects or WT defects treated with PBS or 2 μg FGF-18 revealed a significant increase of healing with FGF-18 treatment as compared with PBS control at 7 day postoperatively. Moreover, there was a trend to increased healing with FGF-18 as compared with untreated WT defects; however, this was not significant, *$p < 0.05$. Color images available online at www.liebertonline.com/tea

this work, we investigated the role of *Fgf-18* in bone regeneration, predicated on the severe impairment of the skeletal system of *Fgf-18* knock out mice. Bone regeneration, but not proliferation or angiogenesis, was severely impaired in *Fgf-18*$^{+/-}$ mice, accompanied by downregulation of *Runx2* and *Osteocalcin*. Other pro-osteogenic *Fgf-* ligands or *Bmp-2* could not compensate for the haploinsufficency of *Fgf-18*; however, it was possible to rescue the tibial defects with FGF-18 protein.

The role of *Fgf-18* in osteogenesis is not fully elucidated; however, there is substantial evidence for its relevance in promoting maturation and proliferation of osteoblasts from both developmental and *in vitro* studies. For instance, it has been previously reported that the osteogenic markers *Osteopontin* and *Osteocalcin* are decreased in embryonic long bones of *Fgf-18*$^{-/-}$ mice.[5,6] Moreover, the expression of *Runx2* was reduced in the trabecular bone, but not in the perichondrium/periosteum and endosteum of *Fgf-18*$^{-/-}$ mice,[6] suggesting that *Fgf-18* is upstream of *Runx2* and that it may be involved in osteoblast maturation. On the contrary, *in vitro* data indicated that forced expression of *Runx2* augmented the expression of *Fgf-18* through canonical Wnt-signaling.[19] Our data suggest that *Fgf-18* is an important mediator of osteogenesis since we demonstrated decreased expression of *Runx2* during bone regeneration in *Fgf-18*$^{+/-}$ mice compared with WT. This observation suggests that perhaps a reciprocal loop between *Runx2* and *Fgf-18* may exist in concurring and promoting osteoblast differentiation. Moreover, results obtained by TRAP staining suggest that Fgf-18 may also play a functional role during late stage of osteogenesis and its turnover.

Despite questions about genes interacting with *Fgf-18*, it remains unclear through which receptors FGF-18 ligand triggers osteogenic differentiation. For instance, in *Stat1*$^{-/-}$ mice, which develop increased bone mass, protein levels of FGF-18 were increased in osteoblasts lining trabecular femoral bone, whereas levels of FGFR-3 were decreased,[23] suggesting that FGF-18 may act independently of FGFR-3. Further, it has been proposed that osteogenic differentiation of murine mesenchymal cells in the presence of dexamethasone is dependent on FGF-18 triggering signal through FGFR-1 and R-2, but not R-3.[24] Indeed, it will be of interest to investigate in our model system through which receptors Fgf-18 is signaling.

It has been reported by Shimoaka *et al.* that *in vitro* FGF-18 induced osteoblast proliferation in a dose-dependent manner, similarly to FGF-2.[25] Moreover, FGF-18 stimulated osteoclast function.[25] In contrast to our *in vivo* data, the authors found that *in vitro* FGF-18 had an inhibitory effect on osteogenic differentiation[25]; however, these data are not consistent with the *in vivo* role described for *Fgf-18*.[5,6] It must be pointed out that similar discrepancies between the *in vivo* and *in vitro* osteogenic effect has also been described for other Fgf ligands.[21,26–29]

An interesting observation emerging from our study was the different effect of *Fgf-18* haploinsufficiency on the phenotype of long bone repair compared with what was previously observed in *Fgf-9* haploinsufficiency.[15] Unlike defects in *Fgf-9*$^{+/-}$ mice, angiogenesis was not impaired in *Fgf-18*$^{+/-}$ tibial defects. Moreover, cell proliferation was impaired in *Fgf-9*$^{+/-}$ but not *Fgf-18*$^{+/-}$ mice. However, it was possible to rescue the defects in both *Fgf*-haploinsufficient mice by treatment with the corresponding protein. It is noteworthy that application of VEGFA to defects created in *Fgf-18*$^{+/-}$ mice did not accelerate healing, whereas this effect was promptly observed in *Fgf-9*$^{+/-}$ mice. These distinct results strongly indicate that angiogenesis was neither a target nor a limiting step in *Fgf-18*$^{+/-}$ tibial defects. The observation that *Fgf-18*$^{+/-}$ mice did not exhibit marked impairment either of angiogenesis or *Vegfa* expression upon bone injury is in agreement with data obtained from one of the original developmental studies by Liu and colleagues showing no differences in the expression level of *Vega* and *Mmp9* genes between E15.5 *Fgf-18*$^{-/-}$ and WT embryos.[6] Therefore, our observation strengths the concept that tissue regeneration recapitulates developmental programs.

Interestingly, we found that temporal endogenous expression of other Fgf ligands, such as *Fgf-2* and *Fgf-9*, could not compensate for the lack of *Fgf-18*. Initial endogenous expression levels of *Fgf-2* and *Fgf-9* were lower in *Fgf-18*$^{+/-}$ mice than WT, but expression was similar to WT at postoperative days 3 and 5. The coincidence of angiogenesis and expression of *Fgf-9* in *Fgf-18*$^{+/-}$ mice at postoperative day 3 further supports the role of *Fgf-9* as an important initial trigger for angiogenesis.[15] Although *Fgf-9* and *Fgf-18* share some functional redundancy during limb development,[4] the effects we observed upon bone regeneration were distinct, indicating that both individual growth factors are required to allow sufficient bone regeneration.

In conclusion, we revealed that *Fgf-18* is required for sufficient bone regeneration. Reduced levels of *Fgf-18* resulted in downregulation of *Runx2* and *Osteocalcin* gene expression upon bone healing, whereas neither cell proliferation nor angiogenesis was affected. The above results provide new aspects of the complex biology of bone repair in the context of FGF-mediated signaling. Collectively, the data gathered from this study and a previous study[15] highlight a distinct but yet converging role of two different Fgf ligands, such as FGF-9 and – 18 in promoting bone repair. Moreover, the study provides valuable hints on how to achieve efficiently programmed bony tissue regeneration in injured long bone.

Acknowledgments

The authors would like to thank Dr. David Ornitz (Washington University, St. Louis, MO) for providing *Fgf-18*$^{+/-}$ mice. This work was supported by the Oak Foundation, NIH R21DE019274 and NIH R01DE019434 to M.T.L., and the German Research Foundation (DFG BE 4169-1) to B.B.

Disclosure Statement

No competing financial interests exist.

References

1. Schindeler, A., McDonald, M.M., Bokko, P., and Little, D.G. Bone remodeling during fracture repair: the cellular picture. Semin Cell Dev Biol **19,** 459, 2008.
2. Gerstenfeld, L.C., Cullinane, D.M., Barnes, G.L., Graves, D.T., and Einhorn, T.A. Fracture healing as a post-natal developmental process: molecular, spatial, and temporal aspects of its regulation. J Cell Biochem **88,** 873, 2003.
3. Montero, A., Okada, Y., Tomita, M., Ito, M., Tsurukami, H., Nakamura, T., *et al.* Disruption of the fibroblast growth

factor-2 gene results in decreased bone mass and bone formation. J Clin Invest **105,** 1085, 2000.
4. Hung, I.H., Yu, K., Lavine, K.J., and Ornitz, D.M. FGF9 regulates early hypertrophic chondrocyte differentiation and skeletal vascularization in the developing stylopod. Dev Biol **307,** 300, 2007.
5. Ohbayashi, N., Shibayama, M., Kurotaki, Y., Imanishi, M., Fujimori, T., Itoh, N., *et al.* FGF18 is required for normal cell proliferation and differentiation during osteogenesis and chondrogenesis. Genes Dev **16,** 870, 2002.
6. Liu, Z., Xu, J., Colvin, J.S., and Ornitz, D.M. Coordination of chondrogenesis and osteogenesis by fibroblast growth factor 18. Genes Dev **16,** 859, 2002.
7. Davidson, D., Blanc, A., Filion, D., Wang, H., Plut, P., Pfeffer, G., *et al.* Fibroblast growth factor (FGF) 18 signals through FGF receptor 3 to promote chondrogenesis. J Biol Chem **280,** 20509, 2005.
8. Jabs, E.W., Li, X., Scott, A.F., Meyers, G., Chen, W., Eccles, M., *et al.* Jackson-Weiss and Crouzon syndromes are allelic with mutations in fibroblast growth factor receptor 2. Nat Genet **8,** 275, 1994.
9. Bellus, G.A., Gaudenz, K., Zackai, E.H., Clarke, L.A., Szabo, J., Francomano, C.A., *et al.* Identical mutations in three different fibroblast growth factor receptor genes in autosomal dominant craniosynostosis syndromes. Nat Genet **14,** 174, 1996.
10. Wilkie, A.O. Craniosynostosis: genes and mechanisms. Hum Mol Genet **6,** 1647, 1997.
11. Shiang, R., Thompson, L.M., Zhu, Y.Z., Church, D.M., Fielder, T.J., Bocian, M., *et al.* Mutations in the transmembrane domain of FGFR3 cause the most common genetic form of dwarfism, achondroplasia. Cell **78,** 335, 1994.
12. Rousseau, F. Mutations in the gene encoding fibroblast growth factor receptor-3 in achondroplasia. Nature **371,** 252, 1994.
13. Bellus, G.A., McIntosh, I., Smith, E.A., Aylsworth, A.S., Kaitila, I., Horton, W.A., *et al.* A recurrent mutation in the tyrosine kinase domain of fibroblast growth factor receptor 3 causes hypochondroplasia. Nat Genet **10,** 357, 1995.
14. Schmid, G.J., Kobayashi, C., Sandell, L.J., and Ornitz, D.M. Fibroblast growth factor expression during skeletal fracture healing in mice. Dev Dyn **238,** 766, 2009.
15. Behr, B., Leucht, P., Longaker, M.T., and Quarto, N. Fgf-9 is required for angiogenesis and osteogenesis in long bone repair. Proc Natl Acad Sci U S A **107,** 11853, 2010.
16. Hinoi, E., Bialek, P., Chen, Y.T., Rached, M.T., Groner, Y., Behringer, R.R., *et al.* Runx2 inhibits chondrocyte proliferation and hypertrophy through its expression in the perichondrium. Genes Dev **20,** 2937, 2006.
17. Hu, M.C., Qiu, W.R., Wang, Y.P., Hill, D., Ring, B.D., Scully, S., *et al.* FGF-18, a novel member of the fibroblast growth factor family, stimulates hepatic and intestinal proliferation. Mol Cell Biol **18,** 6063, 1998.
18. Ohbayashi, N., Hoshikawa, M., Kimura, S., Yamasaki, M., Fukui, S., and Itoh, N. Structure and expression of the mRNA encoding a novel fibroblast growth factor, FGF-18. J Biol Chem **273,** 18161, 1998.
19. Reinhold, M.I., and Naski, M.C. Direct interactions of Runx2 and canonical Wnt signaling induce FGF18. J Biol Chem **282,** 3653, 2007.
20. Bolland, B.J., Kanczler, J.M., Dunlop, D.G., and Oreffo, R.O. Development of *in vivo* muCT evaluation of neovascularisation in tissue engineered bone constructs. Bone **43,** 195, 2008.
21. Quarto, N., and Longaker, M.T. FGF-2 inhibits osteogenesis in mouse adipose tissue-derived stromal cells and sustains their proliferative and osteogenic potential state. Tissue Eng **12,** 1405, 2006.
22. Street, J., Bao, M., deGuzman, L., Bunting, S., Peale, F.V., Jr., Ferrara, N., *et al.* Vascular endothelial growth factor stimulates bone repair by promoting angiogenesis and bone turnover. Proc Natl Acad Sci U S A **99,** 9656, 2002.
23. Xiao, L., Naganawa, T., Obugunde, E., Gronowicz, G., Ornitz, D.M., Coffin, J.D., *et al.* Stat1 controls postnatal bone formation by regulating fibroblast growth factor signaling in osteoblasts. J Biol Chem **279,** 27743, 2004.
24. Hamidouche, Z., Fromigue, O., Nuber, U., Vaudin, P., Pages, J.C., Ebert, R., *et al.* Autocrine fibroblast growth factor 18 mediates dexamethasone-induced osteogenic differentiation of murine mesenchymal stem cells. J Cell Physiol **224,** 509, 2010.
25. Shimoaka, T., Ogasawara, T., Yonamine, A., Chikazu, D., Kawano, H., Nakamura, K., *et al.* Regulation of osteoblast, chondrocyte, and osteoclast functions by fibroblast growth factor (FGF)-18 in comparison with FGF-2 and FGF-10. J Biol Chem **277,** 7493, 2002.
26. Canalis, E., Centrella, M., and McCarthy, T. Effects of basic fibroblast growth factor on bone formation *in vitro*. J Clin Invest **81,** 1572, 1988.
27. Mansukhani, A., Bellosta, P., Sahni, M., and Basilico, C. Signaling by fibroblast growth factors (FGF) and fibroblast growth factor receptor 2 (FGFR2)-activating mutations blocks mineralization and induces apoptosis in osteoblasts. J Cell Biol **149,** 1297, 2000.
28. Nagai, H., Tsukuda, R., and Mayahara, H. Effects of basic fibroblast growth factor (bFGF) on bone formation in growing rats. Bone **16,** 367, 1995.
29. Behr, B., Panetta, N.J., Longaker, M.T., and Quarto, N. Different endogenous threshold levels of Fibroblast Growth Factor-ligands determine the healing potential of frontal and parietal bones. Bone **47,** 281, 2010.

Address correspondence to:
Michael T. Longaker, M.D., M.B.A.
Hagey Laboratory
Department of Surgery
Stanford University School of Medicine
257 Campus Drive
Stanford, CA 94305

E-mail: longaker@stanford.edu

Natalina Quarto, Ph.D.
Hagey Laboratory
Department of Surgery
Stanford University School of Medicine
257 Campus Drive
Stanford, CA 94305

E-mail: quarto@unina.it

Received: December 14, 2010
Accepted: April 1, 2011
Online Publication Date: May 26, 2011